IEEE Access
Multidisciplinary | Rapid Review | Open Access Journal

Received 24 August 2022, accepted 14 September 2022, date of publication 20 September 2022,
date of current version 30 September 2022.

Digital Object Identifier 10.1109/ACCESS.2022.3208106

RESEARCH ARTICLE

Reconfigurable Model Predictive Control for Grid Connected PV Systems Using Thirteen-Level Packed E-Cell Inverter

ABDELBASET LAIB[1], ABDELBASSET KRAMA[2], (Member, IEEE), ABDESLEM SAHLI[1], ABBES KIHAL[1], AND HAITHAM ABU-RUB[2], (Fellow, IEEE)

[1]Independent Researcher, Setif 19000, Algeria
[2]Electrical and Computer Engineering Department, Texas A&M University at Qatar, Doha, Qatar

Corresponding author: Abdelbasset Krama (krama.abdelbasset@qatar.tamu.edu)

This work was supported in part by the Qatar National Research Fund (a member of Qatar Foundation) under Grant NPRP12S-0226-190158, and in part by the Open Access Funding through the Qatar National Library. The statements made herein are solely the responsibility of the authors.

ABSTRACT This paper describes a novel single-phase thirteen-level packed E-cell inverter (PEC13) for grid-tied photovoltaic (PV) systems. PEC13 topology contains six power switches, two four-quadrant switches and four DC capacitors. The main advantage offered by the proposed PEC13 is the ability to produce different voltage levels without any modifications in power circuit when open circuit fault occurs on one or two four-quadrant switches. In faulty condition, PEC13 can continue its operation and behaves as PEC9 or PUC7 inverter configuration. Furthermore, a reconfigurable finite-control set model predictive control (R-FCS-MPC) is designed to control the proposed grid-connected PV systems based PEC13 inverter. The proposed R-FCS-MPC assures the transition between PEC13 to PEC9 or PUC7 configuration through the adjustment of DC-link capacitor voltages balancing. The effectiveness of the R-FCS-MPC with the proposed PEC13 topology is evaluated through experimental validations using real-time hardware in the loop (HIL) setup. Provided experimental results demonstrate that the R-FCS-MPC enables to achieve the normal operation, multi-functionality, besides the high performance of the novel PEC13 inverter topology under step change in solar irradiance and faulty operation of four-quadrant switches.

INDEX TERMS Photovoltaic system, thirteen-level packed E-Cell (PEC13), grid-connected multilevel inverter, finite-control set model predictive control (FCS-MPC).

I. INTRODUCTION

The utilization of fossil fuels as a major global energy source to meet the increase of world's electricity demand has caused environmental crises such as air pollution and greenhouse impact [1], [2], [3], [4]. Therefore, renewable energy resources, such as solar, wind, biomass and hydraulic energies have given great attention in order to minimize the drawbacks caused by the use of fossil fuel [1], [2], [3], [4], [5]. Solar energy has become an energy resource of most interest due to its many special advantages such as wide availability, suitability in various locations, zero carbon emissions, sustainability, and low maintenance requirement [5].

To exploit this energy resource, the photovoltaic (PV) systems can be connected to the main grid or operate in islanded mode feeding a local load. These two operating modes have been investigated in several research works during the last years in order to increase the entire system efficiency and reliability under various operation conditions [5]. To achieve high power quality in the grid-connected PV systems, the multilevel inverters (MLIs) are widely investigated [6]. MLIs offer many advantages such as low switching frequency, small grid-side filter, low voltage stress across semiconductor switches and less total harmonic distortion in the output voltage and current as compared with the two-level inverter [6].

The associate editor coordinating the review of this manuscript and approving it for publication was Ali Raza.

Many conventional MLIs topologies, such as cascaded H-bridge (CHB), neutral point clamp (NPC) and flying capacitor (FC) are widely used in different industrial applications including uninterruptible power supply, conveyor systems, fans, renewable energy systems, active power filters, etc [7], [8]. However, the number of power electronics components increases intensely with the number of output voltage levels which causes the increase of MLIs cost [6]. To overcome this drawback, several researchers strived to design new MLIs with less power electronic components by employing diverse combinations of active switches, isolated DC source and other passive components [9].

The design of new topologies highly depends on the combination of conventional structures [9]. For example, hybrid multilevel inverter (HMLI) with low switching devices and capacitors based-on cascad H-bridge features has been presented in [8]. Furthermore, NPC and FC inverters have been integrated to design the active NPC (ANPC) inverter [10]. Moreover, asymmetrical cascaded HB has been integrated with NPC or conventional two-level inverter as presented in [11] and [12] in order to enhance the energy efficiency and to decrease the switching frequency operation of high-voltage cell. These hybrid topologies produce a higher number of voltage levels and provide higher efficiency [8], [12].

By combining the FC and CHB conveniences, a novel family of single DC source inverter namely, Packed U-Cell (PUC) inverter was developed and employed as an individual cell in [13]. PUC topology was designed to achieve five-level output voltage or seven-level by using only six switches and one DC capacitor. Because of these benefits, the PUC converter has been given significant attention and has been employed in many applications [14]. Vahedi *et al.* have worked on modifying the topology of PUC inverter while keeping the same number of components to make it suitable for active power filtering application [15]. Furthermore, Jagabar Sathik *et al.* have proposed an improved PUC inverter with a voltage boosting capability [16]. The proposed topology in [17] is developed using one DC capacitor and nine power switches to produce seven-level voltage at the output and to increase the output voltage levels generated by PUC inverter. Sharifzadeh *et al.* have tended to replace the U-Cell of packed structure in PUC inverter by E-Cell. Consequently, the PEC topology could produce nine-level output voltage via one four-quadrant switch, six active switches and two DC capacitors [18]. PEC topology with a suitable designed controller has the ability to generate different numbers of voltage levels without any changes in power circuit when an open-circuit fault occurs in the four-quadrant switch. However, the unbalance of DC-link capacitor voltages is considered as the major weaknesses of PUC structure likewise the other MLIs structures [19]. For this reason, the control scheme design becomes more challenging as long as the output voltage levels is increased. Thus, a comprehensive comparison was conducted with several recently developed inverters. The outcome of this comparison is summarized in Table. 1.

TABLE 1. Comparison of several recently developed inverters.

	Levels	switches	Four quadrant switch	Diodes	DC sources	DC capacitors	Reconfigurable capability
PUC7 [11]	7	6	0	0	1	1	No
MPUC7 [13]	7	6	0	0	1	1	No
IPUC7 [15]	7	9	0	0	1	1	No
CSCMLI [16]	9	9	1	0	1	2	No
PEC9 [17]	9	6	1	0	1	2	Yes
Proposed topology	13	6	2	0	1	4	Yes

Voltage-oriented control (VOC) has been commonly explored in the literature for grid-tied MLIs [19], [20]. To apply this technique, PI regulators are necessary in the inner current loops in addition to a modulation stage based-on pulse width modulation (PWM) or space vector modulation (SVM) in the outer loop [19], [20]. To design the modulation stage for MLIs, the DC-link capacitor voltages balancing is required, which increase the complexity of the control algorithm [21]. Furthermore, PI controller drawbacks including sluggish response and high overshoot/undershoot under sudden change of operating conditions, reduces the performance of the power converter. Due to rapid expansion of signal processor capabilities and digital control platforms, the VOC is modified using an advanced control strategies such as sliding mode control (SMC) [22], and model predictive control (MPC) [23]. These methods eliminate the drawbacks caused by the inner PI regulators. However, the design of modulation stage including DC-link capacitors voltage balancing is of need.

Recently, finite-control set model predictive control (FCS-MPC) has been intensively used for power converters control [24], [25]. FCS-MPC gets rid of the PI regulators and modulation stage; meanwhile it has the capability to include system nonlinearities and constraints in the control objective [26]. Due to its simplicity, FCS-MPC has been employed to control MLIs for numerous applications such as AC motor drives, high-voltage direct current (HVDC), flexible AC transmission systems (FACTS), medium and high voltage power applications [8], [9]. Furthermore, FCS-MPC includes DC-link capacitor voltages unbalancing issue in the control objective, while providing higher control performance in comparison with the conventional controllers [27], [28], [29].

Taking the advantage of replacing the U-Cell in PUC structure by E-Cell that was proposed firstly in [18] for nine level, a new single-phase thirteen-level packed E-cell inverter (PEC13) for grid-connected PV systems is proposed in this paper. PEC13 topology is composed of six power switches, two four-quadrant switches and four DC capacitors. The interesting advantage of the suggested topology lies in its capability to generate different numbers of voltage levels without any changes in power circuit when an open-circuit fault occurs on one or two four-quadrant switches. In such case, the PEC13 inverter can continue its operation by switching to either PEC9 or PUC7. To assure the switching between these structures, the adjustment of DC-link capacitor voltages

balancing should be performed which increases the complexity of control design. For this reason, FCS-MPC is adopted to design reconfigurable FCS-MPC (R-FCS-MPC) algorithm for the suggested topology.

To assess the effectiveness of the proposed control with the proposed PEC13 topology, a series of experimental tests are conducted via HIL testing platform. The suggested control scheme is tested under irradiance changes and under four-quadrant switch faulty operations to show the normal and multi-functional operation of the suggested PEC13 inverter.

The reminder of the paper is arranged as follows: the thirteen-level PEC inverter-based grid-tied PV system is discussed in section 2. Section 3 is devoted to the PEC13 inverter topology and its switching sequences. The reconfigurable finite-control-set model predictive control for grid-tied PEC13 inverter is described in section 4. While, section 5 discusses the proposed reconfigurable MPC for grid-tied PEC13 inverter. HIL implementation results are presented and discussed in section 6. Finally, section 7 summarizes the results of this work and draws conclusions.

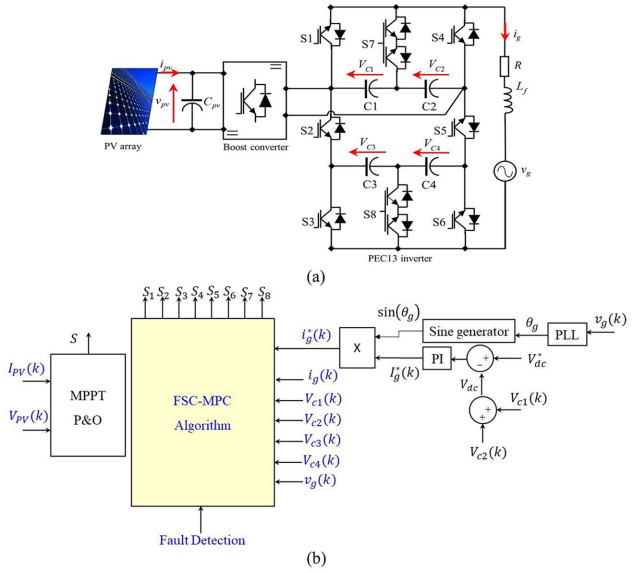

FIGURE 1. Proposed system: (a) power circuit configuration, (b) control scheme.

II. THIRTEEN LEVEL PEC INVERTER BASED GRID-CONNECTED PV SYSTEM

The proposed structure of thirteen-level PEC inverter-based grid-connected PV system and its control structure, are presented in Fig. 1. The investigated system involves PV array, DC/DC boost converter and thirteen-level PEC inverter tied to a single AC source through R, L filter. The main goal of this structure is to inject the produced PV power into the AC network with high quality of grid current even under solar irradiance variation. As exhibited in Fig. 1, the control system is composed of the following:

1) A voltage oriented MPPT based on PI controller presented in [30] is used to track the maximum power point produced by the PV array during solar irradiance variations.
2) A conventional PI regulator is used to regulate the DC-link voltage and to generate the peak of grid current reference, where the PI controller parameters ($K_p = -0.19$ and $K_i = -2.1$) are estimated using the method presented in [31].
3) Proposed R-FCS-MPC control strategy, which is designed for thirteen-level PEC inverter operating in grid-connection mode.

III. THIRTEEN LEVEL PEC INVERTER TOPOLOGY

Recently, few research works have been introduced E-Cell topology to replace the U-Cells in order to set up new multilevel inverters with less components [18], [32], [33]. In this regard, a PEC13 topology is developed in this paper for grid connected PV system with less electronic devices. The suggested PEC13 topology contains six active bidirectional current devices S_1, S_2, S_3, S_4, S_5 and S_6; two four-quadrant switches $S7$, $S8$, four capacitors C_1, C_2, C_3, and C_4 to design thirteen-level single-phase inverter topology, as illustrated in Fig. 1. In PEC13 configuration, each four-quadrant switch is tied between the inverter AC terminal and the midpoint of two capacitors.

To generate thirteen-voltage level V_{in} at the AC terminal by PEC13 inverter, the capacitor voltages V_{c_1} and V_{c_2} must be balanced to half of the input DC voltage magnitude E, while V_{c_3} and V_{c_4} have to be balanced at one sixth using the redundant switching states. Table. 2 clarifies the eighteen possible switching states of the proposed PEC13 inverter while, Fig. 2 shows the switching configurations for generating the thirteen voltage levels.

The proposed PEC13 topology is considered as a reliable configuration, where, it has the ability to generate different number of voltage levels without any further adaptation to the power circuit. When an open-circuit fault occurs on one or two four-quadrant switches, PEC13 can continue its operation by generating nine or seven output voltage levels. Consequently, the capacitors C_1, C_2 and C_3, C_4 are considered as one equivalent capacitor C_{eq} with half the value of C_1 and C_2 or C_3 and C_4 since they are connected in series.

In case of open-circuit fault on four-quadrant device S_8, the PEC13 can continue its operation as PEC9 topology by generating nine-level voltage at the AC terminal. Where, the capacitors C_3 and C_4 are considered as one equivalent capacitor C_{eq_2} with half the value of C_3 and C_4 because they are coupled in series. In this case, the capacitor voltages V_{c_1} and V_{c_2} should be balanced to half of the input DC voltage magnitude E, while the sum of V_{c_3} and V_{c_4} is balanced to one quarter of E using the redundant switching states. The proposed PEC13 topology generates twelve switching states in order to produce the preferred nine-level voltage as presented in Table. 3.

In addition, the proposed PEC13 configuration can operate as another PEC9 structure during an open-circuit fault arises on four-quadrant switch S_7. Meanwhile, the capacitors C_1

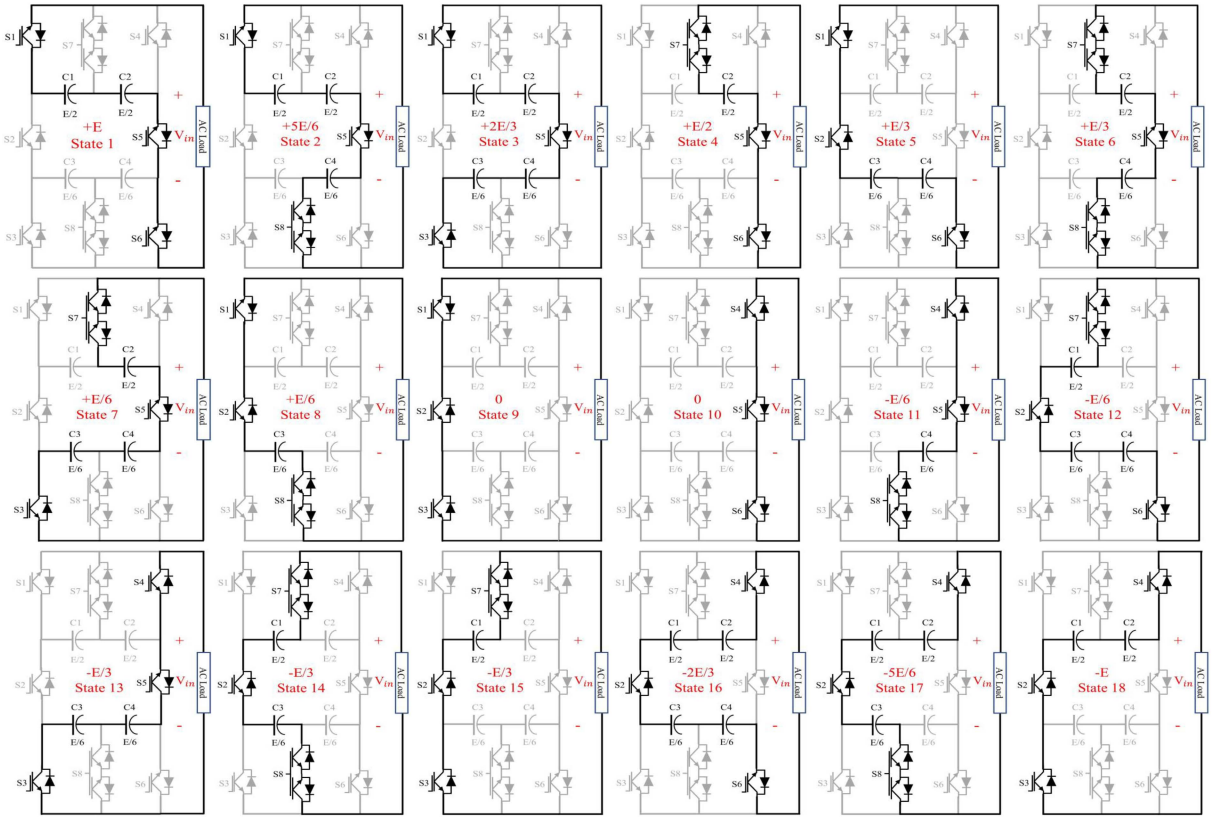

FIGURE 2. Switching states of the proposed PEC 13 inverter.

and C_2 are considered as one equivalent capacitor C_{eq1} with half the value of C_1 and C_2 because they are connected in series. To generate nine-level voltage at the inverter output, the V_{c_3} and V_{c_4} should be balanced to one quarter of the input DC voltage magnitude E via the redundant switching states. Whilst, the sum of capacitor voltages V_{c_1} and V_{c_2} is regulated to the magnitude of input DC voltage E. As presented in Table. 4, twelve possible switching states can be produced by the PEC13 inverter to generate the preferred nine-level voltage.

When a fault occurs on the two four-quadrant devices S_7 and S_8, the PEC13 inverter will be operating as PUC7 topology. Consequently, the capacitors C_1 and C_2 are considered as one equivalent capacitor C_{eq_1} with half the value of C_1 and C_2. Furthermore, the capacitors C_3 and C_4 are also considered as one equivalent capacitor C_{eq2} with half the value of C_3 and C_4. The sum of DC capacitor voltages V_{c_1} and V_{c_2} is regulated to the magnitude of the input DC voltage E while the sum of V_{c_3} and V_{c_4} is balanced to one third. The eight possible switching states of PEC13 inverter topology during PUC7 structure operation are illustrated in Table. 5.

TABLE 2. Switching states of PEC13 inverter topology during normal operation.

Inverter output voltage V_{in}	S_1	S_2	S_3	S_4	S_5	S_6	S_7	S_8
$V_{c1}+V_{c2}=+E$	1	0	0	0	1	1	0	0
$V_{c1}+V_{c2}-V_{c4}=+5E/6$	1	0	0	0	1	0	0	1
$V_{c1}+V_{c2}-V_{c3}-V_{c4}=+2E/3$	1	0	1	0	1	0	0	0
$V_{c2}=+E/2$	0	0	0	0	1	1	1	0
$V_{c3}+V_{c4}=+E/3$	1	1	0	0	0	1	0	0
$V_{c2}-V_{c4}=+E/3$	0	0	0	0	1	0	1	1
$V_{c2}-V_{c3}-V_{c4}=+E/6$	0	0	1	0	1	0	1	0
$V_{c3}=+E/6$	1	1	0	0	0	0	0	1
0	1	1	1	0	0	0	0	0
0	0	0	0	1	1	1	0	0
$-V_{c4}=-E/6$	0	0	0	1	1	0	0	1
$V_{c3}+V_{c4}-V_{c1}=-E/6$	0	1	0	0	0	1	1	0
$-V_{c4}-V_{c3}=-E/3$	0	0	1	1	1	0	0	0
$V_{c3}-V_{c1}=-E/3$	0	1	0	0	0	0	1	1
$-V_{c1}=-E/2$	0	1	1	0	0	0	1	0
$V_{c3}+V_{c4}-V_{c1}-V_{c2}=-2E/3$	0	1	0	1	0	1	0	0
$V_{c3}-V_{c1}-V_{c2}=-5E/6$	0	1	0	1	0	0	0	1
$-V_{c1}-V_{c2}=-E$	0	1	1	1	0	0	0	0

IV. MODEL PREDICTIVE CONTROL FOR GRID-TIED PEC13 INVERTER

Recently, the FCS-MPC is widely introduced to design effective control schemes for the complicated multilevel inverters. Thus, FCS-MPC easily allows including the balance of the DC-link capacitors voltages in the control objective unlike

TABLE 3. Switching states of PEC13 inverter topology during first PEC9 structure operation.

Inverter output voltage V_{in}	S_1	S_2	S_3	S_4	S_5	S_6	S_7
$V_{c1}+V_{c2}=+E$	1	0	0	0	1	1	0
$V_{c1}+V_{c2}-(V_{c3}+V_{c4})=+3E/4$	1	0	1	0	1	0	0
$V_{c2}=+E/2$	0	0	0	0	1	1	1
$V_{c2}-(V_{c3}+V_{c4})=+E/4$	0	0	1	0	1	0	1
$V_{c3}+V_{c4}=+E/4$	1	1	0	0	0	1	0
0	1	1	1	0	0	0	0
0	0	0	0	1	1	1	0
$-(V_{c3}+V_{c4})=-E/4$	0	0	1	1	1	0	0
$(V_{c3}+V_{c4})-V_{c1}=-E/4$	0	1	0	0	0	1	1
$-V_{c1}=-E/2$	0	1	1	0	0	0	1
$V_{c3}+V_{c4}-V_{c1}-V_{c2}=-3E/4$	0	1	0	1	0	1	0
$-V_{c1}-V_{c2}=-E$	0	1	1	1	0	0	0

TABLE 4. Switching states of PEC13 inverter topology during second PEC9 structure operation.

Inverter output voltage V_{in}	S_1	S_2	S_3	S_4	S_5	S_6	S_8
$V_{c1}+V_{c2}=E$	1	0	0	0	1	1	0
$V_{c1}+V_{c2}-V_{c4}=+3E/4$	1	0	0	0	1	0	1
$(V_{c1}+V_{c2})-(V_{c3}+V_{c4})=+E/2$	1	0	1	0	1	0	0
$V_{c3}+V_{c4}=+E/2$	1	1	0	0	0	1	0
$V_{c3}=+E/4$	1	1	0	0	0	0	1
0	1	1	1	0	0	0	0
0	0	0	0	1	1	1	0
$-V_{c4}=-E/4$	0	0	0	1	1	0	1
$(V_{c3}+V_{c4})-(V_{c1}+V_{c2})=-E/2$	0	1	0	1	0	1	0
$-(V_{c3}+V_{c4})=-E/2$	0	0	1	1	1	0	0
$-(V_{c1}+V_{c2})+V_{c3}=-3E/4$	0	1	0	1	0	0	1
$-(V_{c1}-V_{c2})=-E$	0	1	1	1	0	0	0

TABLE 5. Switching states of PEC13 inverter topology during PUC7 structure operation.

Inverter output voltage V_{in}	S_1	S_2	S_3	S_4	S_5	S_6
$V_{c1}+V_{c2}=+E$	1	0	0	0	1	1
$(V_{c1}+V_{c2})-(V_{c3}+V_{c4})=+2E/3$	1	0	1	0	1	0
$(V_{c3}+V_{c4})=+E/3$	1	1	0	0	0	1
0	1	1	1	0	0	0
0	0	0	0	1	1	1
$-(V_{c3}+V_{c4})=-E/3$	0	0	1	1	1	0
$-(V_{c1}+V_{c2})+(V_{c3}+V_{c4})=-2E/3$	0	1	0	1	0	1
$-(V_{c1}+V_{c2})=-E$	0	1	1	1	0	0

classical control schemes [6]. In this section, FCS-MPC for the proposed PEC13 inverter is designed according to the conventional MPC presented in [26] in order to achieve the following objectives:

1) Control the grid current under sudden irradiation change.
2) Ensure the balancing of the DC-link capacitor voltages.

The dynamic model of the grid tied PEC13 inverter is necessary to design the FCS-MPC. According to Fig. 1, the mathematical modelling of the grid current is expressed as [26]

$$L\frac{di_g(t)}{dt} = V_{in} - v_g - Ri_g \tag{1}$$

where i_g and v_g are the grid current and voltage respectively, while V_{in} is the PEC13 inverter output voltage which can be written as

$$V_{in} = F_1V_{c_1} + F_2V_{c_2} + F_3V_{c_3} + F_4V_{c_4} \tag{2}$$

where F_1, F_2, F_3 and F_4 can be calculated based on switching states of PEC13 as follows

$$\begin{cases} F_1 = (S_1\bar{S}_2\bar{S}_4S_5\bar{S}_7) - (\bar{S}_1S_2\bar{S}_5) \\ F_2 = (\bar{S}_2\bar{S}_4S_5) - (\bar{S}_1S_2S_4\bar{S}_5\bar{S}_7) \\ F_3 = (S_2\bar{S}_3\bar{S}_5) - (\bar{S}_2S_3S_5\bar{S}_6\bar{S}_8) \\ F_4 = (S_2S_3\bar{S}_5S_6\bar{S}_8) - (\bar{S}_2S_5\bar{S}_6) \end{cases} \tag{3}$$

By using Euler forward method to discretize the continuous model presented in (1), the discrete model of grid current in terms of the sampling time T_s, is described as [26]

$$i_g(k+1) = (1 - \frac{RT_s}{L})i_g(k) + \frac{T_s}{L}(V_{in}(k) - v_g(k)) \tag{4}$$

The mathematical model of the DC-link capacitor voltages is expressed in terms of the DC-link capacitor currents i_cx and grid current i_g as follows

$$\begin{cases} i_1 = C_1\dfrac{dv_{c_1}}{dt} = -F_1i_g \\ i_2 = C_2\dfrac{dv_{c_2}}{dt} = -F_2i_g \\ i_3 = C_3\dfrac{dv_{c_3}}{dt} = -F_3i_g \\ i_4 = C_4\dfrac{dv_{c_4}}{dt} = -F_4i_g \end{cases} \tag{5}$$

The discretization of (5) can be given as [26]

$$\begin{cases} V_{c_1}(k+1) = V_{c_1}(k) - F_1\dfrac{T_s}{C_1}i_g(k) \\ V_{c_2}(k+1) = V_{c_2}(k) - F_2\dfrac{T_s}{C_2}i_g(k) \\ V_{c_3}(k+1) = V_{c_3}(k) - F_3\dfrac{T_s}{C_3}i_g(k) \\ V_{c_4}(k+1) = V_{c_4}(k) - F_4\dfrac{T_s}{C_4}i_g(k) \end{cases} \tag{6}$$

The objectives of FCS-MPC are comprised in the cost function g as

$$\begin{aligned} g = {} & |i_g^* - i_g(k+1)| + \lambda[|V_{c_1}(k+1) - V_{c_2}(k+1)| \\ & + |V_{c_1}(k+1) - 3V_{c_3}(k+1)| \\ & + |V_{c_1}(k+1) - 3V_{c_4}(k+1)| \\ & + |V_{c_2}(k+1) - 3V_{c_3}(k+1)| \\ & + |V_{c_2}(k+1) - 3V_{c_4}(k+1)| \\ & + |V_{c_3}(k+1) - V_{c_4}(k+1)|] \end{aligned} \tag{7}$$

where i_g is the grid current reference estimated by the DC-link voltage PI regulator, while λ is the weighting factor for the DC-link capacitor voltages balancing.

Where λ is identified to achieve a good balancing of the DC-link capacitor voltages based on the guidelines presented in [34]. However, selecting a large value for λ provides a good DC-link capacitor voltages balancing, but with undesirable tracking errors. On the other hand, a low value for λ leads to a drift in the DC-link capacitor voltages. An appropriate arrangement is to estimate the λ value such that the drift in DC-link capacitor voltages does not exceed 5% of the nominal DC-link capacitor voltages.

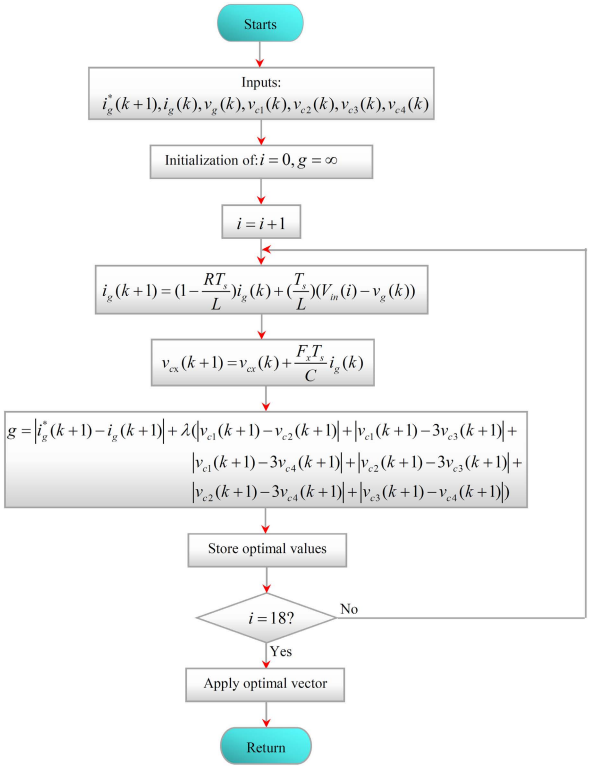

FIGURE 3. Model predictive control for PEC13 during normal operation.

The flowchart presented in Fig. 3 demonstrates the basic operation of the suggested FCS-MPC for the grid-tied PEC13 inverter. From the measured grid current and voltage, the future behaviors of grid current and DC-link capacitor voltages are calculated using (4) and (6) respectively. Then, a cost function g is assessed for the eighteen switching states of PEC13 topology. The switching state that minimizes the cost function is selected and applied during the next sampling time.

V. RECONFIGURABLE FCS-MPC FOR GRID-TIED PEC13 INVERTER

As detailed in section 3, the proposed PEC13 topology has the ability to generate nine or seven-level voltage without modifying the power circuit when an open-circuit fault arises on one or two four-quadrant switches. This feature is achievable only if the control scheme is adjusted to generate the corresponding switching states of the desired voltage levels. For this reason, the FCS-MPC algorithm is designed in a way to enable multiple operation of the PEC13 including thirteen, nine or seven voltages level generation. To achieve these operation modes using FCS-MPC, a proper calculation of the inverter output voltage, the future DC-link capacitor voltage behavior and a cost function are required. Besides, the thirteen-level operating mode presented in section 4, the other three operating modes are discussed bellow.

1) FIRST CONFIGURATION OF PEC9 INVERTER

When a four-quadrant switch S_8 experiences open-circuit fault, PEC13 is able to produce nine voltage levels. The inverter output voltage can be rewritten as follows

$$V_{in} = F_1 V_{c1} + F_2 V_{c3} + F_3 V_{ceq_2} \tag{8}$$

where $V_{ceq_2} = V_{c_3} + V_{c_4}$ while F_1, F_2 and F_3 are given based on switching states illustrated in Table. 2 as follows

$$\begin{cases} F_1 = (S_1\bar{S}_2\bar{S}_4S_5\bar{S}_7) - (\bar{S}_1S_2\bar{S}_5) \\ F_2 = (\bar{S}_2\bar{S}_4S_5) - (\bar{S}_1S_2S_4\bar{S}_5\bar{S}_7) \\ F_3 = (S_2\bar{S}_3\bar{S}_5S_6) - (\bar{S}_2S_3S_5\bar{S}_6) \end{cases} \tag{9}$$

The future behavior of DC-link capacitor voltages is given by

$$\begin{cases} V_{c_1}(k+1) = V_{c_1}(k) - F_1\dfrac{T_s}{C_1} i_g(k) \\ V_{c_2}(k+1) = V_{c_2}(k) - F_2\dfrac{T_s}{C_2} i_g(k) \\ V_{ceq_2}(k+1) = V_{ceq_2}(k) - F_3\dfrac{T_s}{C_{eq_2}} i_g(k) \end{cases} \tag{10}$$

where C_{eq_2} is the equivalent capacitor of C_3 and C_4 connected in series. In order to produce nine output voltage levels during a faulty four-quadrant switch S_8, the cost function g is rewriting as follow

$$\begin{aligned} g = {} & |i_g^* - i_g(k+1)| + \lambda[|V_{c_1}(k+1) - V_{c_2}(k+1)| \\ & + |V_{c_1}(k+1) - 2V_{ceq_2}(k+1)| \\ & + |V_{c2}(k+1) - 2V_{ceq_2}(k+1)|] \end{aligned} \tag{11}$$

2) SECOND CONFIGURATION OF PEC9 INVERTER

The PEC13 can also generate nine voltage levels in case of faulty four-quadrant switch S_7. The inverter output voltage will be expressed as follows

$$V_{in} = F_1 V_{ceq_1} + F_2 V_{c_3} + F_3 V_{c_4} \tag{12}$$

where V_{ceq_1} is the sum of V_{c_1} and V_{c_2} while F_1, F_2 and F_3 are given based on switching states demonstrated in Table. 4 as

$$\begin{cases} F_1 = (S_1\bar{S}_2\bar{S}_4S_5) - (\bar{S}_1S_2S_4\bar{S}_5) \\ F_2 = (\bar{S}_2\bar{S}_3\bar{S}_5) - (\bar{S}_2S_3S_5\bar{S}_6\bar{S}_8) \\ F_3 = (S_2\bar{S}_3\bar{S}_5S_6\bar{S}_8) - (\bar{S}_2S_5\bar{S}_6) \end{cases} \tag{13}$$

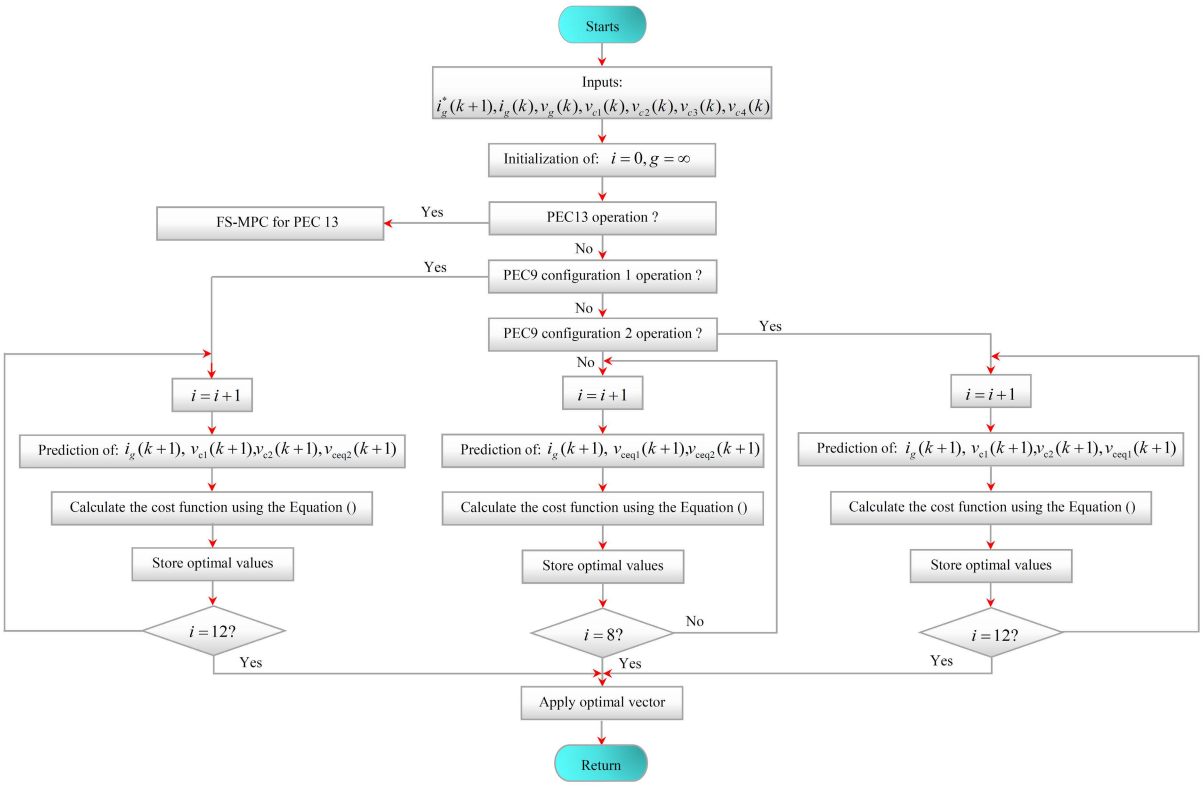

FIGURE 4. Flowchart of reconfigurable model predictive control for the proposed PEC13 topology.

Moreover, the future behavior of DC-link capacitor voltages is given by

$$\begin{cases} V_{ceq_1}(k+1) = V_{ceq_1}(k) - F_1 \dfrac{T_s}{C_{eq_1}} i_g(k) \\ V_{c_3}(k+1) = V_{c_3}(k) - F_2 \dfrac{T_s}{C_3} i_g(k) \\ V_{c_4}(k+1) = V_{c_4}(k) - F_3 \dfrac{T_s}{C_4} i_g(k) \end{cases} \tag{14}$$

where C_{eq_1} is the equivalent capacitor of C_1 and C_2 connected in series. In this case, the cost function g is rewriting to achieve nine output voltage levels as

$$\begin{aligned} g = |i_g^* - i_g(k+1)| + \lambda[&|V_{ceq_1}(k+1) - 4V_{c_3}(k+1)| \\ &+|V_{ceq_1}(k+1) - 4V_{c_4}(k+1)| \\ &+|V_{c_3}(k+1) - V_{c_4}(k+1)|] \end{aligned} \tag{15}$$

3) PUC7 INVERTER CONFIGURATION

In case of faulty four-quadrant switches S_7 and S_8, the PEC13 can operate as PUC7 inverter. Therefore, the output voltage of PUC7 inverter can be described as follows

$$V_{in} = F_1 V_{ceq_1} + F_2 V_{ceq_2} \tag{16}$$

where, $F1$ and $F2$ are given in terms of the switching states illustrated in Table. 5 as

$$\begin{cases} F_1 = (S_1\bar{S}_2\bar{S}_4S_5) - (\bar{S}_1S_2S_4\bar{S}_5) \\ F_2 = (S_2\bar{S}_3\bar{S}_5S_6) - (\bar{S}_2S_3S_5\bar{S}_6) \end{cases} \tag{17}$$

The future behavior of V_{ceq_1} and V_{ceq_2} are written as

$$\begin{cases} V_{ceq_1}(k+1) = V_{ceq_1}(k) - F_1 \dfrac{T_s}{C_{eq_1}} i_g(k) \\ V_{ceq_2}(k+1) = V_{ceq_2}(k) - F_2 \dfrac{T_s}{C_{eq_2}} i_g(k) \end{cases} \tag{18}$$

The cost function g that assure the PUC7 operation mode is derived as

$$g = |i_g^* - i_g(k+1)| + \lambda[|V_{ceq_1}(k+1) - 3V_{ceq_2}(k+1)|] \tag{19}$$

Fig. 4 presents the flowchart of the proposed reconfigurable FCS-MPC. In the normal operation when S_7 and S_8 are operating properly, the R-FCS-MPC takes into consideration the normal PEC13 operation as presented in Fig. 4. Nevertheless, the R-FCS-MPC turns to operate as FCS-MPC for the first configuration of PEC9 if a fault in four-quadrant switches S_8 is occurred. In this case, the future behaviors of grid current and DC-link capacitor voltages are calculated using (4) and (8-10). Then, a cost function g is evaluated using (11) for all 12 switching states of the first configuration of PEC9 topology. While a fault is occurred on S_7, the R-FCS-MPC turns to work as FCS-MPC for the second configuration of PEC9. The future behaviors of grid current and DC-link capacitor voltages are calculated using (4) and (12-14). Then, a cost function g is evaluated using (11) for all 12 switching states of the second configuration of PEC9 topology.

The R-FCS-MPC turns to work as FCS-MPC for the PUC7 configuration while a fault is occurred on S_7 and S_8. By using (4) and (16-18), the future behavior of grid current and DC-link capacitor voltages are calculated. Then, a cost function g is evaluated using (19) for the 8 switching states of PUC7 topology.

VI. HIL RESULTS

In this section, a laboratory testbed of the entire system based on hardware in the loop (HIL) testing methodology is built around dSPACE 1103 and OPAL-RT 5600 units in order to evaluate the effectiveness of the grid-connected PV system with the proposed PEC13 inverter controlled by the suggested R-FCS-MPC. The HIL testbed components are shown in Fig. 5.

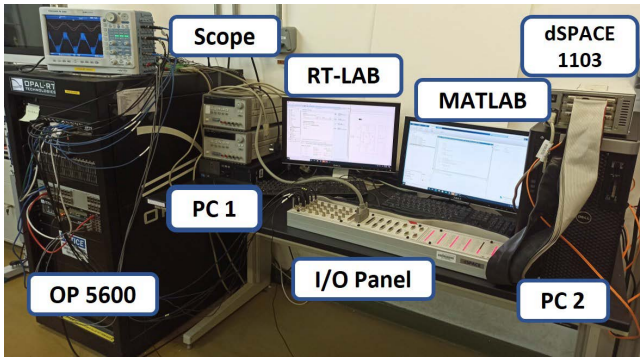

FIGURE 5. HIL setup based on OPAL-RT and dSPACE 1103.

The proposed R-FCS-MPC, P&O MPPT and DC-link PI controller are implemented in dSPACE 1103 real-time controller. On the other hand, the OPAL-RT is used as a real time simulator to simulate the entire power plant including the grid, PV system and the proposed PEC13 power circuit. The real-time simulator based on OPAL-RT offers the ability to simulate the comportment of the power system as fast as would be carried out in the real world with high accuracy. In HIL testbed, the dSPACE receives from the OPAL-RT the actual PV current, PV voltage, DC-link capacitor voltages, grid current and voltage signals through analog-to-digital converter (DAC) channels. Those measurements are used to calculate the optimal control signals via the proposed control scheme and then send them to the OPAL-RT via digital to analog channels as illustrated in Fig. 6.

The OPAL-RT is configured with MATLAB, which communicates with RT-LAB software to generate real-time code. The real-time code is generated by MATLAB in combination with dSPACE real-time blocks and downloaded in dSPACE hardware in order to be executed in real time. The real-time data (PV current, PV voltage, DC-link capacitor voltages, grid current and voltage signals) can be displayed on an oscilloscope by using the DAC channels that are available on the connector panel of the OPAL-RT. The overall system parameters used in real-time HIL testing are listed in Table. 6.

The overall system is first tested under step changes in solar irradiance (from 700 m^2/W to 1000 m^2/W and 1000 m^2/W to 400 m^2/W) in order to present the normal operation performance of the proposed topology. The PV system reaches quickly the new MPP in both cases as shown in Fig. 7.

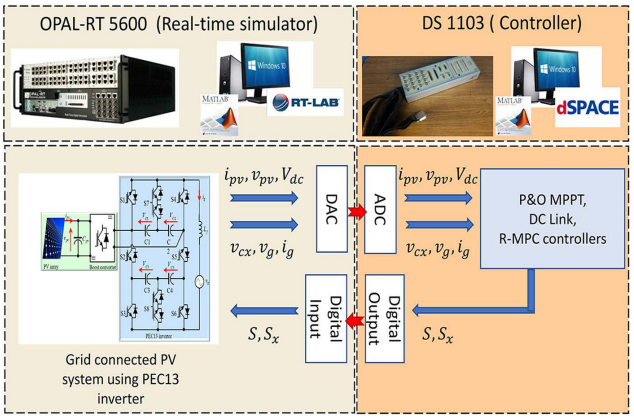

FIGURE 6. HIL diagram for the grid-connected PV system using PEC13 inverter.

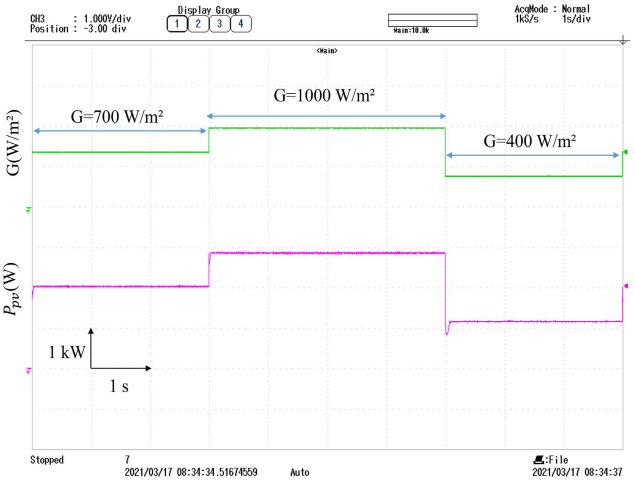

FIGURE 7. Waveforms of solar irradiance and PV power output.

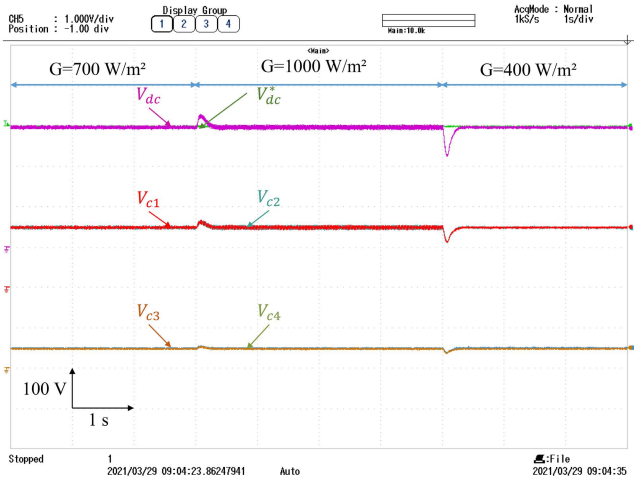

FIGURE 8. Waveforms of DC-link voltage and four DC-link capacitor voltages under solar irradiance changes.

TABLE 6. Overall system parameters.

PV array (Siemens SM110)	Values
Maximum power Pmpp	120 W
Open circuit voltage V_{oc}	42.1 V
Short circuit current I_{sc}	3.87 A
Voltage at Pmax	33.7
Current at Pmax	3.56
Number of cells connected in parallel (N_p)	1
Number of cells connected in series N_s	72
Number of modules connected in series N_{ss}	4
Number of modules connected in parallel N_{pp}	6
Boost converter	**Values**
Inductance L	1 mH
Input capacitance C_{in}	2200 µF
Grid parameters	**Values**
Grid peak Voltage v_g	220 V
Grid Side Inductor L_g	0.1 mH
Grid Side Resistor R_g	0.1 Ω
Grid Frequency f_g	60 Hz
PEC13 inverter parameter	**Values**
DC-link Capacitors $C_1, C_2, C_3 \& C_4$	4700 µF
DC Voltage Reference V_{dcref}	300 V
Filter parameter	**Values**
Filter Side Inductor L_f	3 mH
Sampling Times	**Values**
MPPT P&O sampling Time T_p	1 ms
R-FS-MPC sampling Time T_s	20 µs
PI controller parameters	**Values**
Proportional gain k_p	-0.19
Integral gain k_i	-2.1

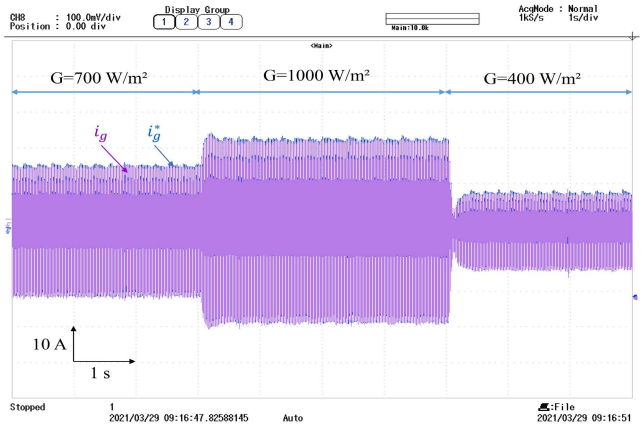

FIGURE 9. Waveform of grid current under solar irradiance changes.

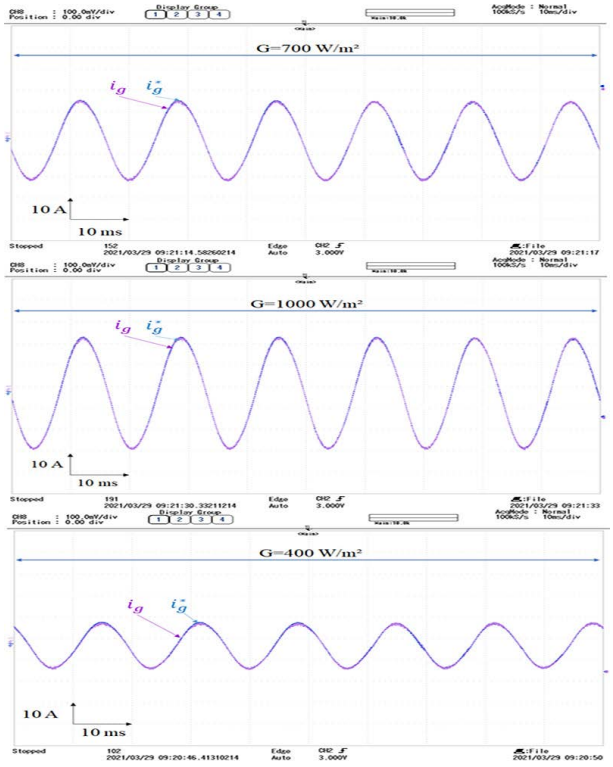

FIGURE 10. Waveform of grid current in several steady state levels.

Moreover, these changes lead to undershoot and overshoot with a small rise time in the V_{dc} over the reference value as displayed in Fig 8. Despite that, the proposed R-FCS-MPC algorithm guarantees a perfect DC-link capacitor voltages balancing as depicted in Fig. 8. Meanwhile, the measured grid current track its reference very well as presented in Figs. 9 and 10.

Fig. 11 shows the waveforms of grid voltage/current under sudden irradiance changes. The grid voltage and current waveforms are in phase, which confirms the unity power factor operation. Fig. 12 depicts the waveforms of grid voltage/current and PEC13 inverter output voltage, which confirms the normal operation of the proposed topology.

Next, the proposed system is tested under faulty four-quadrant switches. The algorithm documented in [35] is employed to detect the open circuit fault occurred in any of the four-quadrant switches. As presented in Fig. 13, the proposed topology is operating in the normal PEC13 mode until a fault in four-quadrant switch S_8 is occurred. At this instant, the proposed inverter switches to operate as PEC9 configuration. The DC-link voltage is maintained at its reference, while the DC-link capacitor voltages change the voltage level balancing to assure nine-level voltage in the inverter output as illustrated in Fig. 13. In addition, the grid current maintains a sinusoidal form and the inverter is well synchronized with the grid voltage as depicted in Figs. 14 and 15. The waveform

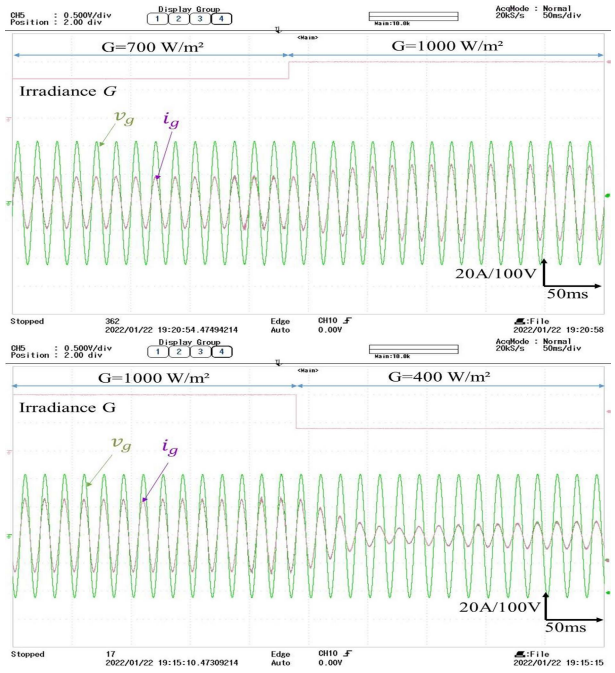

FIGURE 11. Zoom of grid current and voltage waveforms under suden irradiance changes.

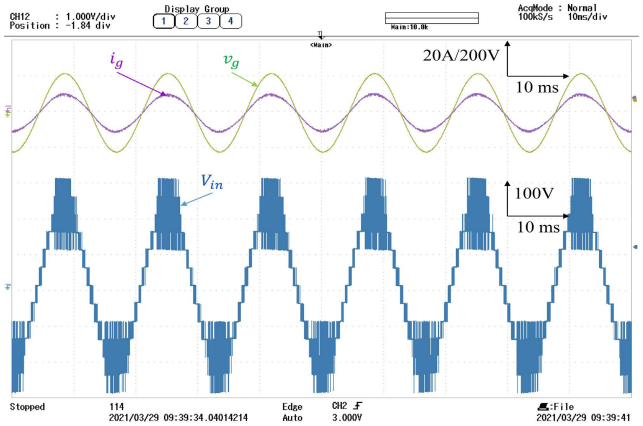

FIGURE 12. Waveforms of grid current, grid voltage and PEC13 output voltage in steady state.

of PEC13 output voltage presented in Fig. 15 demonstrates the both operation modes (PEC13 and first PEC9 structure). In this case, the transition time includes the fault detection and control model shift is about 21 ms.

Then, the suggested inverter topology is operating in the second PEC9 configuration due to the fault occurred in four-quadrant switch S_7. After that, another fault in four-quadrant switch S_8 is occurred as depicted in Fig. 16. The proposed R-FCS-MPC offers the ability to change the operation of the proposed configuration from the second PEC9 configuration to PUC7 configuration. Nine and seven level voltages at the inverter output are assured by achieving a suitable DC-link capacitor voltages balancing while the DC-link voltage is well regulated over its reference as presented in Fig. 16. Moreover, the grid current remained

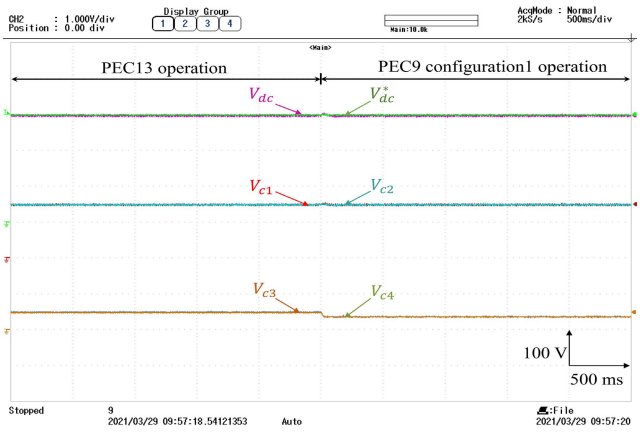

FIGURE 13. Waveforms of DC-link voltage, four DC-link capacitor voltages during a faulty four-quadrant switch S_8.

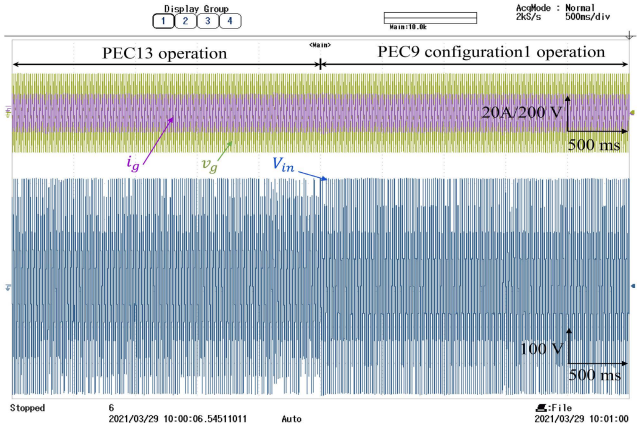

FIGURE 14. Waveforms of grid current, grid voltage, and PEC13 output voltage under a faulty four-quadrant switch S_8.

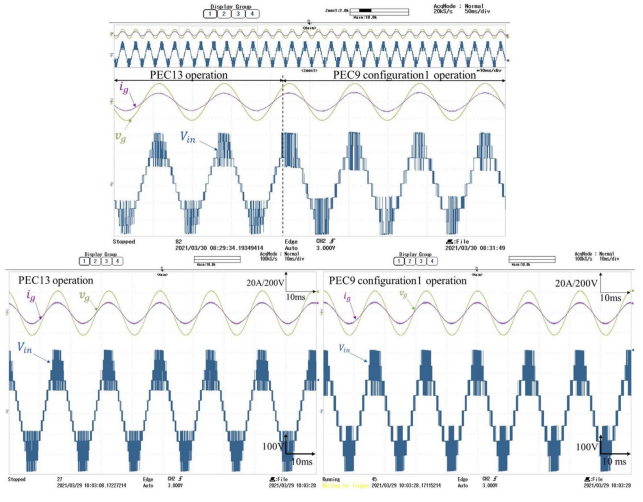

FIGURE 15. Zoom of grid current, grid voltage and PEC13 output voltage under a fault in four-quadrant switch S_8.

sinusoidal and kept in phase with the grid voltage as depicted in Figs. 17 and 18. The operation modes (second PEC9 and PUC7) are demonstrated according to the waveform of PEC13 output voltage presented in Fig. 18. The transition

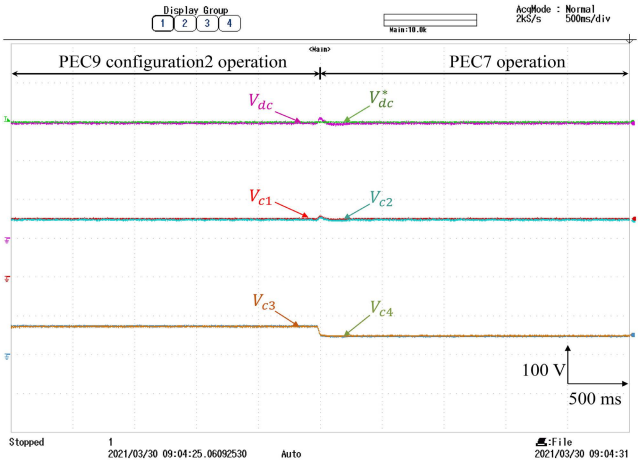

FIGURE 16. Waveforms of DC-link voltage and four DC-link capacitor voltages during a fault in four-quadrant switches S_7 and S_8.

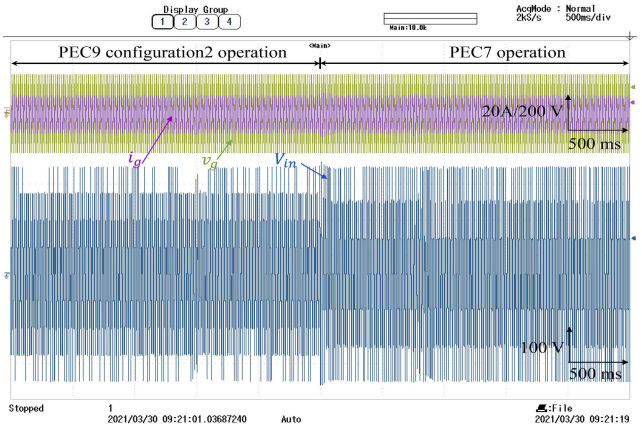

FIGURE 17. Waveforms of grid current, grid voltage and PEC13 output voltage under a fault in four-quadrant switches S_7 and S_8.

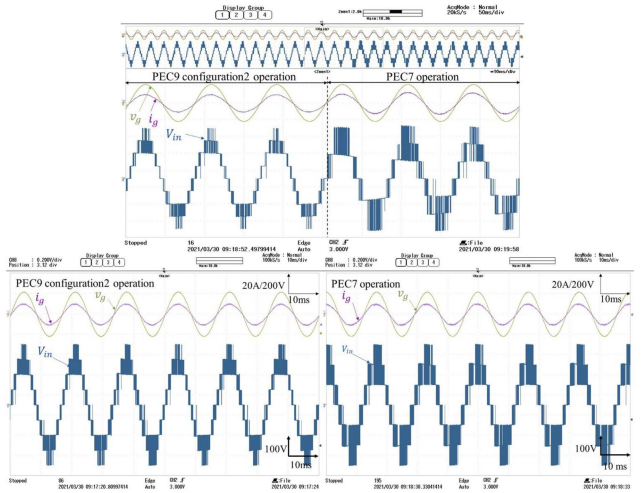

FIGURE 18. Zoom of grid current, grid voltage and PEC13 output voltage under a fault in four-quadrant switches S_7 and S_8.

time from the fault detection and the change between the PEC9 mode to PUC7 mode is about 18 ms.

TABLE 7. Analysis of grid current quality (THD%) under solar irradiance changes and four-quadrant switch faulty operations.

Irradiation $G\ (W/m^2)$	G=700	G=1000	G=400
PEC13 (THDi%)	1.72	1.51	2.22
PEC9 configuration 1 (THDi%)	2.15	1.80	2.99
PEC9 configuration 2 (THDi%)	2.16	1.83	3.13
PUC7 (THDi%)	2.72	2.04	4.04

According to Table. 7, the PEC13 provides high grid current quality in normal operation under full solar irradiance. However, the grid current quality is slightly decreased when a fault in four-quadrant switches is occurred.

Despite that fault, the grid current quality still aligns with the international standards (IEEE-519, $THD < 5\%$) during all operating conditions which confirms the efficiency of the suggested PEC13 structure and R-FCS-MPC controller. On the other hand, the computational time measured while running the R-FCS-MPC controller of the PEC13 including the configurable feature in the OPA-RT was around 6.8 μs, which can be implemented easily in the most of the real-time controllers available in the market.

VII. CONCLUSION

A novel single-phase thirteen-level packed E-cell inverter (PEC13) was proposed and investigated in this paper for grid-connected photovoltaic systems. The proposed topology is composed of six power switches, two four-quadrant switches, and four DC capacitors. Compared with the existing MLI topologies, PEC13 topology offers the ability to generate different numbers of voltage levels without any power circuit modification. This advantage allows the PEC13 topology to operate as two PEC9 operation modes or PUC7 in order to ensure reliable operation during faulty condition that may happen on one or two of four-quadrant switches. To guarantee the direct transition between PEC13 to either PEC9 or PUC7, a reconfigurable finite control set model predictive control (R-FCS-MPC) was properly designed to accomplish this multifunction operation. A series of experimental tests using a hardware in the loop (HIL) testing methodology have been carried out to evaluate the performance of the PEC13 topology with the proposed control scheme based on the reconfigurable finite-control-set model predictive control. The obtained results show that the R-FCS-MPC is enabled to achieve the normal operation, multi-functionality, as well as the high performance of the novel PEC13 inverter topology under step changes in the solar irradiance and four-quadrant switch faulty operations. Moreover, the grid current quality under different solar irradiances and faulty four-quadrant switches meets the international standards (IEEE-519, $THD < 5\%$) which confirms the effectiveness of the proposed inverter structure and control methodology.

REFERENCES

[1] A. Laib, F. Krim, B. Talbi, and A. Sahli, "A predictive control scheme for large-scale grid-connected PV system using high-level NPC inverter," *Arabian J. Sci. Eng.*, vol. 45, no. 3, pp. 1685–1701, 2020.

[2] K. Zeb, W. Uddin, M. A. Khan, Z. Ali, M. U. Ali, N. Christofides, and H. J. Kim, "A comprehensive review on inverter topologies and control strategies for grid connected photovoltaic system," *Renew. Sustain. Energy Rev.*, vol. 94, pp. 1120–1141, Oct. 2018.

[3] M. A. Eltawil and Z. Zhao, "Grid-connected photovoltaic power systems: Technical and potential problems—A review," *Renew. Sustain. Energy Rev.*, vol. 14, no. 1, pp. 112–129, 2010.

[4] R. A. Mastromauro, M. Liserre, T. Kerekes, and A. Dell'Aquila, "A single-phase voltage-controlled grid-connected photovoltaic system with power quality conditioner functionality," *IEEE Trans. Ind. Electron.*, vol. 56, no. 11, pp. 4436–4444, Nov. 2009.

[5] A. Laib, F. Krim, B. Talbi, A. Kihal, and H. Feroura, "Improved control for three phase dual-stage grid-connected PV systems based on predictive control strategy," *J. Control Eng. Appl. Informat.*, vol. 20, no. 3, pp. 12–23, 2018.

[6] H. Aburub, J. Holtz, and J. Rodriguez, "Medium-voltage multilevel converters—State of the art, challenges, and requirements in industrial applications," *IEEE Trans. Ind. Electron*, vol. 57, no. 8, pp. 2581–2596, Dec. 2010.

[7] H. P. Vemuganti, D. Sreenivasarao, S. K. Ganjikunta, H. M. Suryawanshi, and H. Abu-Rub, "A survey on reduced switch count multilevel inverters," *IEEE Open J. Ind. Electron. Soc.*, vol. 2, pp. 80–111, 2021.

[8] Y. Khandelwal, A. Routray, R. K. Singh, and R. Mahanty, "Reduced voltage stress hybrid multilevel inverter using optimised predictive control," *IET Power Electron.*, vol. 13, no. 14, pp. 2983–2991, Nov. 2020.

[9] A. K. Gupta and A. M. Khambadkone, "A space vector PWM scheme for multilevel inverters based on two-level space vector PWM," *IEEE Trans. Ind. Electron.*, vol. 53, no. 5, pp. 1631–1639, Oct. 2006.

[10] W. Sheng and Q. Ge, "A novel seven-level ANPC converter topology and its commutating strategies," *IEEE Trans. Power Electron.*, vol. 33, no. 9, pp. 7496–7509, Sep. 2018.

[11] S. Mariethoz, "Systematic design of high-performance hybrid cascaded multilevel inverters with active voltage balance and minimum switching losses," *IEEE Trans. Power. Electron*, vol. 28, no. 7, pp. 3100–3113, Oct. 2012.

[12] S. Mariéthoz, "Design and control of high-performance modular hybrid asymmetrical cascade multilevel inverters," *IEEE Trans. Ind. Appl.*, vol. 50, no. 6, pp. 4018–4027, Nov./Dec. 2014.

[13] Y. Ounejjar and K. Al-Haddad, "A novel high energetic efficiency multilevel topology with reduced impact on supply network," in *Proc. 34th Annu. Conf. IEEE Ind. Electron.*, Nov. 2008, pp. 489–494.

[14] A. N. Babadi, O. Salari, M. J. Mojibian, and M. T. Bina, "Modified multilevel inverters with reduced structures based on packed U-cell," *IEEE J. Emerg. Sel. Topics Power Electron.*, vol. 6, no. 2, pp. 874–887, Jun. 2017.

[15] H. Vahedi, M. Sharifzadeh, and K. Al-Haddad, "Modified seven-level pack U-cell inverter for photovoltaic applications," *IEEE J. Emerg. Sel. Top. Power Electron*, vol. 6, no. 3, pp. 1508–1516, Apr. 2018.

[16] M. J. Sathik, K. Bhatnagar, N. Sandeep, and F. Blaabjerg, "An improved seven-level PUC inverter topology with voltage boosting," *IEEE Trans. Circuits Syst. II, Exp. Briefs*, vol. 67, no. 1, pp. 127–131, Jan. 2019.

[17] J. S. M. Ali and V. Krishnasamy, "Compact switched capacitor multilevel inverter (CSCMLI) with self-voltage balancing and boosting ability," *IEEE Trans. Power Electron.*, vol. 34, no. 5, pp. 4009–4013, May 2018.

[18] M. Sharifzadeh and K. Al-Haddad, "Packed E-cell (PEC) converter topology operation and experimental validation," *IEEE Access*, vol. 7, pp. 93049–93061, 2019.

[19] N. A. Rahim and J. Selvaraj, "Multistring five-level inverter with novel PWM control scheme for PV application," *IEEE Trans. Ind. Electron.*, vol. 57, no. 6, pp. 2111–2123, Jun. 2009.

[20] K. Rayane, M. Bougrine, A. Krama, A. Benalia, M. Trabelsi, and H. Abu-Rub, "Average model-based feedforward and feedback control for PUC5 inverter," *IEEE Access*, vol. 8, pp. 172962–172971, 2020.

[21] M. Bouzidi, S. Barkat, and A. Krama, "New simplified and generalized three-dimensional space vector modulation algorithm for multilevel four-leg diode clamped converter," *IEEE Trans. Ind. Electron.*, vol. 68, no. 10, pp. 9908–9918, Oct. 2021.

[22] A. Krama, S. S. Refaat, and H. Abu-Rub, "A robust second-order sliding mode control of sensorless five level packed u cell inverter," in *Proc. 46th Annu. Conf. IEEE Ind. Electron. Soc.*, Oct. 2020, pp. 2412–2417.

[23] M. Trabelsi, S. Bayhan, K. A. Ghazi, H. Abu-Rub, and L. Ben-Brahim, "Finite-control-set model predictive control for grid-connected packed-U-cells multilevel inverter," *IEEE Trans. Ind. Electron.*, vol. 63, no. 11, pp. 7286–7295, Nov. 2016.

[24] J. Rodriguez, M. P. Kazmierkowski, J. R. Espinoza, P. Zanchetta, H. Abu-Rub, H. A. Young, and C. A. Rojas, "State of the art of finite control set model predictive control in power electronics," *IEEE Trans. Ind. Informat.*, vol. 9, no. 2, pp. 1003–1016, May 2012.

[25] B. Talbi, F. Krim, T. Rekioua, A. Laib, and H. Feroura, "Design and hardware validation of modified P&O algorithm by fuzzy logic approach based on model predictive control for MPPT of PV systems," *J. Renew. Sustain. Energy*, vol. 9, no. 4, 2017, Art. no. 043503.

[26] M. Bouzidi, S. Barkat, A. Krama, and H. Abu-Rub, "Simplified predictive direct power control of three-phase three-level four-leg grid connected NPC converter," *IEEE Open J. Ind. Electron. Soc.*, vol. 3, pp. 448–459, 2022.

[27] A. Laib, F. Krim, B. Talbi, H. Feroura, and A. Kihal, "Decoupled active and reactive power control strategy of grid-connected six-level diode-clamped inverters based on finite set model predictive control for photovoltaic application," *Revue Roumaine des Sci. Techn.-Serie Electrotechnique et Energetique*, vol. 64, no. 1, pp. 51–56, 2019.

[28] A. Sahli, F. Krim, A. Laib, and B. Talbi, "Energy management and power quality enhancement in grid-tied single-phase PV system using modified PUC converter," *IET Renew. Power Gener.*, vol. 13, no. 14, pp. 2512–2521, Oct. 2019.

[29] H. Abu-Rub, J. Holtz, J. Rodriguez, and G. Baoming, "Medium-voltage multilevel converters—State of the art, challenges, and requirements in industrial applications," *IEEE Trans. Ind. Electron.*, vol. 57, no. 8, pp. 2581–2596, Aug. 2010.

[30] M. A. G. de Brito, L. Galotto, L. P. Sampaio, G. de Azevedo e Melo, and C. A. Canesin, "Evaluation of the main MPPT techniques for photovoltaic applications," *IEEE Trans. Ind. Electron.*, vol. 60, no. 3, pp. 1156–1167, Mar. 2012.

[31] A. Sahli, F. Krim, and A. Belaout, "Energy management and power quality improvement in grid-connected photovoltaic systems," in *Proc. Int. Renew. Sustain. Energy Conf. (IRSEC)*, Dec. 2017, pp. 1–7.

[32] M. Babaie, M. Sharifzadeh, M. Mehrasa, and K. Al-Haddad, "Lyapunov based neural network estimator designed for grid-tied nine-level packed E-cell inverter," in *Proc. IEEE Appl. Power Electron. Conf. Expo. (APEC)*, Mar. 2020, pp. 3311–3315.

[33] N. Guler, H. Komurcugil, S. Bayhan, and S. Biricik, "Current sensorless control strategy for nine-level packed-E-cell rectifier," in *Proc. 47th Annu. Conf. IEEE Ind. Electron. Soc.*, Oct. 2021, pp. 1–6.

[34] P. Cortes, S. Kouro, B. La Rocca, R. Vargas, J. Rodriguez, J. Leon, S. Vazquez, and L. Franquelo, "Guidelines forweighting factors design in model predictive control of power converters and drives," in *Proc. IEEE Int. Conf. Ind. Tech. (ICIT)*, Melbourne, VIC, Australia, Feb. 2009, pp. 1–7.

[35] A. Yazdani, H. Sepahvand, M. L. Crow, and M. Ferdowsi, "Fault detection and mitigation in multilevel converter STATCOMs," *IEEE Trans. Ind. Electron.*, vol. 58, no. 4, pp. 1307–1315, Apr. 2010.

ABDELBASET LAIB received the B.S., M.S., and Ph.D. degrees in electronics and industrial control from the University Ferhat Abbas of Setif, Algeria, in 2011, 2013, and 2019, respectively. In 2021, he was a Postdoctoral Research Associate at the Department of Electrical and Computer Engineering, Texas A&M University at Qatar. He is currently an Independent Researcher. His research interests include nonlinear control, advanced control strategies, multilevel inverters, new converter topologies, control of power converters, reliability of power electronic system, and renewable energy sources. He serves as a reviewer in several IEEE journals and conferences.

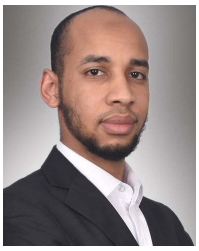

ABDELBASSET KRAMA (Member, IEEE) received the bachelor's and master's (Hons.) degrees in electrical engineering from the Kasdi Merbah University of Ouargla, Ouargla, Algeria, in 2013 and 2015, respectively, and the Ph.D. degree from El Oued University, El Oued, Algeria, in 2019. From 2017 to 2018, he was an Assistant Lecturer at the University of Ouargla. In October 2018, he joined the Department of Electrical and Computer Engineering, Texas A&M University at Qatar, Doha, Qatar, as a Research Assistant, where he was promoted to a Research Associate, in June 2019. Since April 2020, he has been a Postdoctoral Research Associate with the Department of Electrical and Computer Engineering, Texas A&M University at Qatar. Dr. Krama is a Professional Active Member of the IEEE Industrial Electronics Society. He is currently the Secretary of the IEEE-IES Qatar Section Chapter. He was a Recipient of many prestigious national and international awards, such as the Student Excellent Award from Ouargla University, in 2015; the Best Presentation Award from American Algerian Foundation (AUF) in Summer University, in 2018; the Outstanding Research Award from Electrical and Computer Engineering at Texas A&M university at Qatar, in 2021; and the Best Paper Award from SGRE 2022 Conference.

ABDESLEM SAHLI received the Engr. (Hons.), Mag. (Hons.), and D.Sc. degrees in electronics engineering from the University Ferhat Abbas of Setif-1, Sétif, Algeria, in 2009, 2012, and 2021 respectively. He is currently an Independent Researcher. His research interests include power quality, nonlinear control, advanced control strategies, multilevel inverters, new converter topologies, reliability of power electronic systems, and renewable energy conversion. He serves as a reviewer in several IEEE journals and conferences.

ABBES KIHAL received the B.S., M.S., and Ph.D. degrees in electronics and industrial control from the University Ferhat Abbas of Setif, Algeria, in 2012, 2014, and 2019, respectively. His research interests include new converter topologies, control of power converters, reliability of power electronic systems, and renewable energy sources.

HAITHAM ABU-RUB (Fellow, IEEE) received the M.Sc. degree in electrical engineering from Gdynia Maritime University, Gdynia, Poland, in 1990, the Ph.D. degree in electrical engineering from the Gdansk University of Technology, Gdansk, Poland, in 1995, and the second Ph.D. degree in humanities from Gdansk University, Gdansk, in 2004. He is currently a Professor with Texas A&M University at Qatar (TAMUQ). He has research and teaching experiences at many universities in many countries, including Qatar, Poland, Palestine, USA, and Germany. He has served for five years as the Chair of Electrical and Computer Engineering Program with TAMUQ, where he is serving as the Managing Director of the Smart Grid Center. He has authored or coauthored more than 500 journal and conference papers, six books, and six book chapters. His main research interests include power electronic converters, renewable energy systems, electric drives, and smart grid. He was a recipient of many national and international awards and recognitions. He is the Co-Editor in Chief for the IEEE TRANSACTIONS ON INDUSTRIAL ELECTRONICS.